Composites Part B 75 (2015) 73–85

Contents lists available at ScienceDirect

Composites Part B

journal homepage: www.elsevier.com/locate/compositesb

# Mechanical characterization of single-walled carbon nanotubes: Numerical simulation study

N.A. Sakharova [a, *], A.F.G. Pereira [a], J.M. Antunes [a, b], C.M.A. Brett [c], J.V. Fernandes [a]

[a] CEMUC – Department of Mechanical Engineering, University of Coimbra, Rua Luís Reis Santos, Pinhal de Marrocos, 3030-788 Coimbra, Portugal
[b] Escola Superior de Tecnologia de Abrantes, Instituto Politécnico de Tomar, Rua 17 de Agosto de 1808, 2200 Abrantes, Portugal
[c] CEMUC – Department of Chemistry, University of Coimbra, Rua Larga, 3004-535 Coimbra, Portugal

ARTICLE INFO

*Article history:*
Received 18 September 2014
Received in revised form
30 November 2014
Accepted 13 January 2015
Available online 29 January 2015

*Keywords:*
A. Nano-structures
B. Elasticity
B. Mechanical properties
C. Finite element analysis (FEA)
Young's modulus

ABSTRACT

The mechanical behaviour of non-chiral and chiral single-walled carbon nanotubes under tensile and bending loading conditions is investigated. For this purpose, three-dimensional finite element modelling is used in order to evaluate the tensile and bending rigidities and, subsequently, the Young's moduli. It is shown that the evolution of rigidity, tensile and bending, as a function of diameter can be described by a unique function for non-chiral and chiral single-walled nanotubes, i.e. regardless of the index or angles of chirality. A comprehensive study of the influence of the nanotube wall thickness and diameter on the Young's modulus values is also carried out. It is established that the evolution of the Young's modulus as a function of the inverse of the wall thickness follows a quasi-linear trend for nanotubes with diameters larger than 1.085 nm. The current numerical simulation results are compared with data reported in the literature. This work provides a benchmark in relation to ascertaining the mechanical properties of chiral and non-chiral single-walled carbon nanotubes by nanoscale continuum models.



## 1. Introduction

Carbon nanotubes (CNTs) are nanostructures attracting research interest due to their extraordinary mechanical, optical, thermal and electrical properties [1]. The CNTs outstanding physical properties such as strength and lightness enable applications in numerous different fields: chemistry, physics, engineering, materials science. From the point of view of structural application, the high stiffness together with low density indicates use of the CNTs as nanoscale fibres for reinforcement of nanocomposite structures (see, for example, [2–4]). This type of application of carbon nanotubes has required the investigation of their mechanical properties, including their deformation behaviour under different loading conditions.

There are two approaches commonly used to study the mechanical properties and deformation behaviour of CNTs: experimental and computational. For single-walled and multi-walled CNTs, methods for measuring Young's modulus based on *in situ* atomic force microscopy (AFM) and transmission electron microscopy (TEM) techniques have been established [5,6]. Although various experimental studies have been carried out to evaluate the mechanical properties of CNTs, there is inconsistency in the experimental results reported in the literature, owing to the complexity of the characterization of nanomaterials at the atomic scale. The common point in the experimental studies is the evidence of the unparallelled mechanical properties of CNTs. Concerning the accuracy of the values of the CNT mechanical properties that are determined, experimental studies still show a wide scatter of their values. From this point of view, computer simulation for predicting the mechanical properties of CNTs has been considered as a powerful tool, due to the experimental difficulties.

The theoretical approaches for the modelling and characterization of the CNTs behaviour can be divided into three main categories: the atomistic approach, the continuum approach and the nanoscale continuum approach. A comprehensive critical review concerning the modelling of the mechanical behaviour of carbon nanotubes has been undertaken by Rafiee and Moghadam [7]. Hereinafter, a brief assessment of main modelling methodologies is carried out.

Atomistic modelling, used solely during the first years of theoretical studies on CNTs, calculates the positions of atoms based on their interactive forces and boundary conditions (see, for example [8]). Atomistic modelling comprises an *ab initio* approach [9] and

* Corresponding author. Tel.: +351 239790747.
*E-mail address:* nataliya.sakharova@dem.uc.pt (N.A. Sakharova).

http://dx.doi.org/10.1016/j.compositesb.2015.01.014
1359-8368/

molecular dynamics (MD) [10–14]. After this, other atomistic modelling methods, such as tight-binding molecular dynamics (TBMD) [15,16] were developed.

Generally, *ab initio* methods give more accurate results than MD, but they are computationally expensive and only possible to use for a small number of molecules or atoms. Molecular dynamics can be used in large systems and provide good predictions of CNT mechanical properties under different loading conditions, but it is still limited owing to its being very time consuming, especially when long or multi-walled CNTs are simulated. In recent years, the atomistic approaches, due to their big computation cost, have been gradually replaced by continuum approaches, which are at the moment the most indicated for effective computational simulation of large systems.

The basic assumption of the continuum mechanics-based approach consists of the modelling of CNTs as a continuum structure, concerning the distribution of mass, stiffness, etc., i.e. the real discrete structure of the nanotubes is neglected and replaced by a continuum medium. Some authors have explored continuum shell modelling for studying the mechanical behaviour of CNTs [17–20]. However, the atomic characteristics of carbon nanotubes, such as chirality, are not taken into account in the continuous shell approach, and so their effects on the mechanical behaviour of CNTs cannot be captured. To overcome this obstacle, Chang proposed an anisotropic shell model for SWCNTs [21] that can predict some anisotropic effects related to chirality. Besides shell structures, other continuum structures, such as tubes and plates, are employed in continuum approaches. In the models of Sears and Batra [22], and Gupta and Batra [23] the whole single-walled CNT structure was simulated as an equivalent continuum tube. Wang [24] employed the equivalent elastic plate model. Arash and Wang [25] show the advantages of the continuum theory applied to the modelling of shells and plates. However, whatever the type of the continuum modelling approach, the replacement of the whole CNT structure by a continuum element is not a completely satisfactory method to evaluate CNT properties.

The nanoscale continuum modelling (NCM) consists of replacing the carbon–carbon (C–C) bond by a continuum element. As a result, continuum mechanics theories can be used at the nanoscale, i.e. a linkage between molecular configuration and solid mechanics is recognized. NCM is frequently accomplished by finite element modelling. The main approach in NCM consists of considering different elements, such as rod, truss, spring and beam, well described in elasticity theory, to simulate C–C bonds (see, for example, [26–29]). The first NCM model of CNTs was developed by Odegard et al. [26] and consisted of a continuum truss model. The disadvantage of the truss model is the impossibility of describing the CNT mechanical behaviour under torsional load, because the out-of-plane torsion of the C–C bond cannot be taken into account.

Various FEM models where the C–C bonds are simulated using diverse kinds of elastic spring element, such as linear, non-linear, rotational, torsional, have been recently reported [30–37]. Although the use of spring elements is an effective way for simulation of the bond angle variations, the accuracy of the Young's modulus results depends on the choice of the potential function for the calculation of the force constants.

Since Li and Chou [27] linked the interatomic potential energies to the strain energies of an equivalent beam element and established a direct relationship between sectional stiffness parameters and the force field constants, equivalent beam approaches have been successfully used to simulate the mechanical behaviour of CNT, although with different formulations of the inter-atomic molecular potential energies and boundary conditions [28,38–43]. The FE models, which employed beam elements in a three-dimensional (3D) space, developed by Tserpes and Papanikos [26], Papanikos et al. [38] and Avila and Lacerda [39] differ from each other mainly due to the boundary conditions and the method for the Young's modulus calculation. The recent 3D FE model of Lu and Hu [42] used the same formulation for potential energy of covalent system, but considering an elliptical cross-section area of equivalent beam. In another analytical approach developed by Shokrieh and Rafiee [40], the deformations of beam elements were obtained using Castigliano's theorem. In the works of Her [41] and Mohammadpour [43] the modified Morse potential function for the potential energy of the covalent system used to describe non-linear behaviour of C–C bonds was applied. It can be concluded from these studies that nanoscale continuum modelling (NCM) is an adequate modelling technique for predicting CNT mechanical properties and shows results in close agreement with those obtained from MD modelling.

In the present study, the equivalent beam approach is used in order to evaluate the tensile and bending rigidities and, subsequently, Young's modulus of various single-walled carbon nanotubes (SWCNT) structures, as non-chiral (zigzag, $\theta = 0°$, and armchair, $\theta = 30°$) and families of chiral ($\theta = 8.9°; 13.9°; 19.1°$ among others) SWCNTs for a wide range of chiral indices, nanotube length and diameter. A comprehensive study of the influence of the nanotube wall thickness and diameter on the Young's modulus results was carried out. Moreover, the present work provides a benchmark in relation to ascertaining the mechanical properties of chiral and non-chiral SWCNTs by nanoscale continuum models.

## 2. Materials and methods

### 2.1. Atomic structure of SWCNTs

A simple way to describe an SWCNT is as a rolled-up graphene sheet giving rise to a hollow cylinder, the surface of which is composed of hexagonal carbon rings (see, for example [44,45]). The hexagonal pattern is repeated periodically, leading to binding of each carbon atom to three neighbouring atoms by covalent bonds. A schematic illustration of an unrolled hexagonal graphene sheet is shown in Fig. 1. The symmetry of the atomic structure of SWCNTs is characterized by the chirality, which is defined by the chiral vector $\boldsymbol{C_h}$:

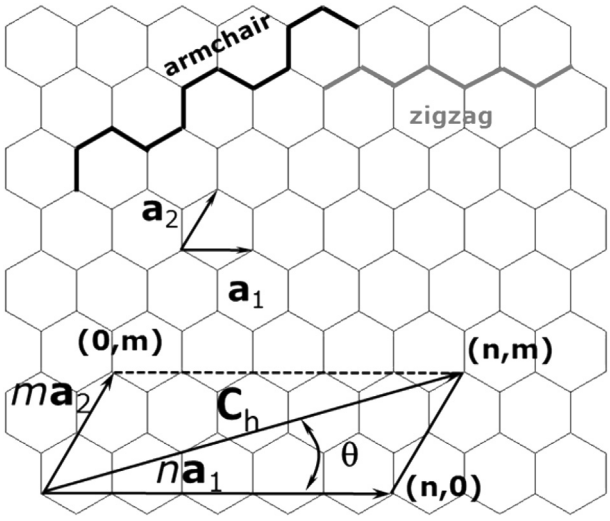


**Fig. 1.** Schematic illustration of an unrolled hexagonal graphene sheet with definition of chiral vector.

$$\boldsymbol{C_h} = n\boldsymbol{a}_1 + m\boldsymbol{a}_2 \quad (1)$$

where *(n,m)* is a pair of the lattice translation indices $\boldsymbol{a}_1$ and $\boldsymbol{a}_2$, the unit vectors of the hexagonal lattice, $n$ and $m$ are integers.

The length of the unit vector $\boldsymbol{a}$ is defined as $a = \sqrt{3}a_{C-C}$ with the equilibrium carbon–carbon (C–C) covalent bond length $a_{C-C}$ usually taken to be 0.1421 nm. The nanotube circumference, $L_c$, and diameter, $D_n$ are defined as:

$$L_c = |\boldsymbol{C_h}| = a\sqrt{n^2 + nm + m^2} \quad (2)$$

$$D_n = \frac{L_c}{\pi} \quad (3)$$

The chiral angle, $\theta$, is the angle between the chiral vector $\boldsymbol{C_h}$ and the direction $(n, 0)$. The chiral angle, $\theta$, is given by Ref. [44]:

$$\theta = \sin^{-1}\frac{\sqrt{3}m}{2\sqrt{n^2 + nm + m^2}} \quad (4)$$

Three main symmetry groups of SWCNTs exist. When $n = m$, the structure *(n, n)* is called the armchair configuration; when $m = 0$, the structure *(n, 0)* is called zigzag; when $n \neq m$, the structure *(n, m)* is called chiral. These three major categories of SWCNTs can also be defined based on the chiral angle, $\theta$. For the two limiting chiral angles of 0° and 30°, the nanotubes are referred to as armchair and zigzag, respectively. For $\theta$ different from 0° and 30°, the nanotubes are designated as chiral [46].

### 2.2. FE modelling of SWCNTs

The displacement of individual carbon atoms in CNT under external forces is constrained by the covalent bonds. Therefore, the overall deformation of the CNT is the result of the interactions between bonds. Since the C–C bonds can be considered as load-carrying elements, and the carbon atoms as joints of connecting elements, it is possible to simulate CNTs as space-frame structures [27,28] and analyze their mechanical behaviour using classical structural mechanics methods.

In the present work, the 3D FE model, which is able to assess the mechanical properties of SWCNTs, proposed in Ref. [28], was adopted. Thus, characterization of the rigidities of SWCNTs is performed based on the equivalent continuum modelling (ECM) approach, where the equivalent beam elements replace the C–C bonds. This approach is based on the premise that the mechanical behaviour of CNTs and elastic beams is identical.

The FE meshes of the carbon nanotube structures used in the finite element analyses were constructed using the academic software CoNTub 1.0 [47], which permits building the CNT structures. This code generates ASCII files, describing atom positions, which can be entered as input in available commercial and in-house FEA codes, in order to perform the simulation of mechanical tests. To convert the ASCII files, obtained using the CoNTub 1.0 program, into the format usable by the commercial FEA code ABAQUS®, the in-house application designated *InterfaceNanotubes* was developed. The FE model uses the coordinates of the carbon atoms for generating the nodes and then the suitable connection of the nodes creates the beam elements. The FE simulation uses the analogy between the bond length, $a_{C-C}$, and the element length L and between the nanotube wall thickness and the element thickness. Assuming the beam element has a circular cross-section area, the wall thickness corresponds to the element diameter.

In the present work, chiral and non-chiral SWCNTs were simulated over a wide range of chiral indices, nanotube lengths and diameters. The FE model takes into account the chirality of the SWCNTs, and so is able to consider their anisotropic behaviour due to chirality. The geometrical characteristics of SWCNTs used for the FE analyses are summarized in Table 1, where the number of nodes and elements of the finite element meshes of the SWCNTs is also indicated for a nanotube with a length of 20 nm. The choice of SWCNT geometrical characteristics was made taking into account real nanotube sizes: for example, the (4, 2) chiral nanotube is the smallest diameter nanotube ever synthesized [48].

Knowledge of the exact dimensions of CNTs at the equilibrium state is still a challenge for research. Unlike the C–C bond length $a_{C-C}$, for which the experimentally observed value of 0.1421 nm is accepted as the exact value, the wall thickness of CNT, $t$, is not clearly specified in the literature. Since in the present study the SWCNTs are modelled as space-frame structures, the wall thickness, $t$, should be identified in a continuum sense. Although a few theoretical reports have provided values for nanotube wall thickness that range from 0.064 [18] to 0.69 nm [26], the most widely used value of 0.34 nm (equal to the interlayer spacing of graphite) is adopted for the SWCNT wall thickness, $t$, in order to enable comparison of the current results with those available in the literature. Nevertheless, taking in account the ambiguity of the value of CNT wall thickness in the literature, a parametric study of the effect of the wall thickness value on the calculation of SWCNT Young's modulus was performed.

### 2.3. FE analysis of SWCNTs

#### 2.3.1. Structural mechanics of SWCNTs

As was originally proposed by Odegard et al. [26], and then developed by Li and Chou [27], the elastic moduli of the beam elements are determined by establishing the link between interatomic potential energies of the molecular structure and strain energies of the equivalent continuum structure comprising of frame members (beams) undergoing axial and bending deformations. From a molecular point of view, the CNTs can be envisaged as large molecules composed of carbon atoms. The force-field is expressed in the form of the total potential energy, which is uniquely defined by the relative positions of the nuclei composing the molecule. According to molecular dynamics, the total empirical inter-atomic potential energy of a molecular system is expressed as a sum of the individual energy terms due to bonded and non-bonded interactions [49]:

$$U_{tot} = \sum U_r + \sum U_\theta + \sum U_\phi + \sum U_\omega + \sum U_{vdw} \quad (5)$$

where $U_r$, $U_\theta$, $U_\phi$, $U_\omega$ are energies associated with bond stretching, bending (bond angle variation), dihedral angle torsion, out-of plane torsion, respectively, and $U_{vdw}$ is the energy associated with non-bonded van der Waals interaction.

Generally, in covalent system, non-bonded interactions are negligible in comparison with bonded ones, and the main contribution to the total potential energy is from the first four terms of Eq. (5). The contributions of dihedral angle torsion and out-of plane torsion to total inter-atomic potential energy are insignificant, compared with contributions of other bonded interactions, and the main contribution to the inter-atomic potential energy is due to bond stretching. Consequently, under the assumption of small deformation, the total inter-atomic potential energy can be approximated by Ref. [50]:

$$U_r = \frac{1}{2}k_r(\Delta r)^2 \quad (6)$$

$$U_\theta = \frac{1}{2}k_\theta(\Delta\theta)^2 \quad (7)$$

**Table 1**
Geometrical characteristics of SWCNTs studied and number of nodes and elements of the finite element meshes used (nanotube length 20 nm).

| SWCNT type | | | $(n, m)$ | $D_n$, nm | $\theta^\circ$ | Number of nodes | Number of elements |
|---|---|---|---|---|---|---|---|
| Non-chiral | Armchiar | | (3, 3) | 0.407 | 30 | 972 | 1448 |
| | | | (5, 5) | 0.678 | | 1620 | 2414 |
| | | | (6, 6) | 0.814 | | 1944 | 2897 |
| | | | (8, 8) | 1.085 | | 2592 | 3863 |
| | | | (9, 9) | 1.221 | | 2916 | 4346 |
| | | | (10, 10) | 1.356 | | 3240 | 4829 |
| | | | (12, 12) | 1.628 | | 3888 | 5795 |
| | | | (15, 15) | 2.034 | | 4860 | 7244 |
| | | | (20, 20) | 2.713 | | 6840 | 9659 |
| | Zigzag | | (3, 0) | 0.235 | 0 | 558 | 830 |
| | | | (5, 0) | 0.392 | | 930 | 1384 |
| | | | (10, 0) | 0.783 | | 1860 | 2769 |
| | | | (12, 0) | 0.940 | | 2232 | 3323 |
| | | | (15, 0) | 1.175 | | 2790 | 4154 |
| | | | (18, 0) | 1.409 | | 3348 | 4985 |
| | | | (20, 0) | 1.566 | | 3720 | 5539 |
| | | | (24, 0) | 1.879 | | 4464 | 6647 |
| Chiral | Family $\theta$ 8.9 | | (5, 1) | 0.436 | 8.9 | 1044 | 1554 |
| | | | (10, 2) | 0.872 | | 2088 | 3109 |
| | | | (15, 3) | 1.308 | | 3132 | 4664 |
| | | | (20, 4) | 1.744 | | 4176 | 6219 |
| | | | (25, 5) | 2.180 | | 5220 | 7774 |
| | | | (30, 6) | 2.616 | | 6264 | 9329 |
| | Family $\theta$ 13.9 | | (6, 2) | 0.565 | 13.9 | 1352 | 2013 |
| | | | (9, 3) | 0.847 | | 2028 | 3020 |
| | | | (12, 4) | 1.129 | | 2740 | 4027 |
| | | | (15, 5) | 1.412 | | 3380 | 5034 |
| | | | (18, 6) | 1.694 | | 4056 | 6041 |
| | | | (21, 7) | 1.976 | | 4732 | 7048 |
| | | | (24, 8) | 2.259 | | 5408 | 8055 |
| | | | (27, 9) | 2.541 | | 6084 | 9062 |
| | Family $\theta$ 19.1 | | (4, 2) | 0.414 | 19.1 | 992 | 1477 |
| | | | (6, 3) | 0.622 | | 1488 | 2216 |
| | | | (8, 4) | 0.829 | | 1984 | 2955 |
| | | | (10, 5) | 1.036 | | 2840 | 3694 |
| | | | (12, 6) | 1.243 | | 2976 | 4433 |
| | | | (14, 7) | 1.450 | | 3472 | 5172 |
| | | | (16, 8) | 1.657 | | 3968 | 5911 |
| | | | (18, 9) | 1.865 | | 4464 | 6650 |
| | | | (20, 10) | 2.072 | | 4960 | 7389 |
| | | | (22, 11) | 2.279 | | 5456 | 8128 |
| | | | (24, 12) | 2.486 | | 5952 | 8867 |
| | $n + m$ | 12 | (7, 5) | 0.818 | 24.5 | 1960 | 2920 |
| | | | (11, 1) | 0.903 | 4.3 | 2167 | 3222 |
| | | 18 | (16, 2) | 1.338 | 5.8 | 3208 | 4777 |
| | | | (14, 4) | 1.282 | 12.2 | 3072 | 4575 |
| | | | (13, 5) | 1.260 | 15.6 | 3020 | 4498 |
| | | | (11, 7) | 1.231 | 22.7 | 2950 | 4395 |
| | | | (10, 8) | 1.223 | 26.3 | 2932 | 4369 |
| | | 24 | (22, 2) | 1.806 | 4.3 | 4328 | 6445 |
| | | | (19, 5) | 1.717 | 11.4 | 4116 | 6130 |
| | | | (17, 7) | 1.674 | 16.5 | 4012 | 5976 |
| | | | (15, 9) | 1.644 | 21.8 | 3942 | 5873 |
| | | | (14, 10) | 1.635 | 24.5 | 3920 | 5841 |
| | | | (13, 11) | 1.629 | 27.2 | 3906 | 5821 |

where $k_r$, $k_\theta$, are the bond stretching and bond bending force constants, respectively, and $\Delta r$ and $\Delta\theta$ are the respective bond stretching and bond angle variation increments.

The interatomic potential energy of the molecular structure comprises bond stretching and angle variation. Thus, the structural member for substituting the C–C bond has to be able to capture both axial and bending deformations. The beam is identified by the cross sectional area, elastic modulus, moment of inertia and length.

Relationships between the sectional stiffness parameters in structural mechanics and force field constants in molecular dynamics are required for the determination of the elastic modulus of beam elements. Thus, the elastic moduli can be determined by establishing the equivalence between the energies associated with the interatomic interactions (through Eqs. (6) and (7)) and with the deformation of the structural elements (i.e. beams) of the space-frame structure.

Classical mechanics gives the following expression for the strain energy of a uniform beam of length, $l$, and cross-section area, $A_b$, under a pure axial force, $N$:

$$U_A = \frac{1}{2}\int_0^L \frac{N^2}{E_b A_b} dl = \frac{1}{2}\frac{N^2\, l}{E_b A_b} = \frac{1}{2}\frac{E_b A_b}{l}(\Delta l)^2 \tag{8}$$

where $\Delta l$ is the axial stretching deformation, and $E_b$ is the Young's modulus of the beam.

The strain energy of a uniform beam, with moment of inertia, $I_b$, under a pure bending moment, $M$, according to classical mechanics, is expressed as:

$$U_M = \frac{1}{2}\int_0^L \frac{M^2}{E_b I_b} dl = \frac{1}{2}\frac{E_b I_b}{l}(2\alpha)^2 \tag{9}$$

where $\alpha$ is the rotational angle at the ends of the beam.

The parameters $U_r$ and $U_A$ are stretching energies in molecular and structural systems, respectively, and $U_\theta$ and $U_M$ represent the corresponding bending energies. Comparing Eqs. (6) and (7) with Eqs. (8) and (9), and assuming the equivalences of the rotational angle, $2\alpha$, with the total variation of the bond angle, $\Delta\theta$, and of $\Delta l$ with $\Delta r$, direct relationships can be established between the structural mechanics parameters, $E_bA_b$, $E_bI_b$, and the force field constants, $k_r$, $k_\theta$, [27]:

$$\frac{E_b A_b}{l} = k_r, \tag{10}$$

$$\frac{E_b I_b}{l} = k_\theta, \tag{11}$$

where $l$ is the bond length generally considered equal to 0.1421 nm. Consequently, Eqs. (10) and (11) establish the basis for application of continuum mechanics to the analysis of the mechanical behaviour of CNTs. In order to determine the rigidities of beam elements, the relationships between the sectional stiffness parameters and force-field constants need to be clarified. In the approach of Li and Chou [27], a solid circular cross-sectional area of the beams with diameter $d$ is assumed and so the geometrical parameters $A_b$ and $I_b$ are as follows:

$$A_b = \frac{\pi d^2}{4} \tag{12}$$

$$I_b = \frac{\pi d^4}{64} \tag{13}$$

Assuming these settings, Eqs. (10) and (11) become, respectively:

$$d = 4\sqrt{\frac{k_\theta}{k_r}} \tag{14}$$

$$E_b = \frac{k_r^2 l}{4\pi k_\theta} \tag{15}$$

Eqs. (14) and (15) allow determining the necessary input parameters for the beam elements. In this study, the bond stretching and bond bending force constants used [51] are:

$$k_r = 6.52 \times 10^{-7}\ \text{N/nm}$$

$$k_\theta = 8.76 \times 10^{-10}\ \text{N nm rad}^{-2}$$

Then, substituting these values in Eqs. (14) and (15) and setting $l = a_{C-C} = 0.1421$ nm, the input parameters for the FE model are obtained. The geometrical and material parameters and values necessary for the finite element simulation of SWCNTs are summarized in Table 2.

**Table 2**
Input parameters for FE simulations of SWCNTs.

| Parameter | Value | Formulation |
|---|---|---|
| C–C bond/beam length ($l = a_{C-C}$) | 0.1421 nm | – |
| Diameter (d) | 0.147 nm | $d = 4\sqrt{k_\theta/k_r}$ |
| Cross section area, $A_b$ | 0.01688 nm$^2$ | $A_b = \pi d^2/4$ |
| Moment of inertia, $I_b$ | $2.269 \times 10^{-5}$ nm$^4$ | $I_b = \pi d^4/64$ |
| Young's modulus, $E_b$ | 5488 GPa | $E_b = k_r^2 l/4\pi k_\theta$ |
| Rigidity, $E_bA_b$ | 92.65 nN | $E_bA_b = k_r l$ |
| Rigidity, $E_bI_b$ | 0.1245 nN nm$^2$ | $E_bI_b = k_\theta l$ |

*2.3.2. Loading conditions*

Numerical simulation of conventional mechanical tension and bending tests was carried out in order to study the effect of nanotube length and diameter on their mechanical properties, focussing on the tensile and bending rigidities. The FE analysis was performed using the commercial FE code ABAQUS®.

In order to simulate the mechanical behaviour of SWCNT in tension, an axial force, $F_x$, is applied at one nanotube end, leaving the other end fixed. The tensile rigidity of the nanotube, $EA$, is determined as:

$$EA = \frac{F_x L}{u_x} \tag{16}$$

where $L$ is the nanotube length and $u_x$ is an axial displacement taken from the FE analysis.

Likewise, for simulating bending, a transverse force, $F_y$, is applied at one extremity of the nanotube, leaving the other fixed. The bending rigidity of the nanotube, $EI$, is determined as:

$$EI = \frac{F_y L^3}{3u_y} \tag{17}$$

where $u_y$ is a transverse displacement taken from the FE analysis.

*2.3.3. Evaluation of the Young's modulus of SWCNTs*

The nanotube rigidities, $EA$ and $EI$, are required for the evaluation of the SWCNT Young's modulus, $E$. Considering a hollow cylindrical profile for the equivalent beam, i.e. a geometry similar to the CNT, the cross-sectional area of the equivalent hollow cylinder and moment of inertia can be written as:

$$A = \frac{\pi}{4}\left[(D+t)^2 - (D-t)^2\right] = \pi D t \tag{18}$$

$$I = \frac{\pi}{64}\left[(D+t)^4 - (D-t)^4\right] \tag{19}$$

where $D$ and $t$ are the mean diameter and the thickness of the equivalent hollow cylinder, respectively.

Assuming $t = t_n$ (where $t_n$ is the nanotube wall thickness), the expression for $D$ can be derived from Eqs. (18) and (19):

$$\frac{EI}{EA} = \frac{1}{8}\left(D^2 + t_n^2\right) \Rightarrow$$

$$D = \sqrt{8\left(\frac{EI}{EA}\right) - t_n^2} \tag{20}$$

Thus, the Young's modulus of the SWCNT can be calculated using the following expression, taking into account the rigidities in tension and bending:

$$E = \frac{EA}{A} = \frac{EA}{\pi t_n \sqrt{8\left(\frac{EI}{EA}\right) - t_n^2}} \quad (21)$$

## 3. Results and discussion

### 3.1. Rigidities of SWCNTs

#### 3.1.1. Effect of the SWCNT's length on the tensile and bending rigidities

The common length of carbon nanotubes currently produced is in the order of 1 μm, their diameter being in the range 0.5–3 nm. Consequently, the modelling of CNT with their real length leads to high computing costs. As is known from previous studies [38], the modelling of real nanotube length is not crucial because of its length-independent mechanical behaviour, with the exception of very small lengths. A study for estimating the minimum length above which the values of the tensile and bending rigidities become stable was performed in order to make a selection of the minimum modelling length of the CNTs.

Examples of the evolution of tensile, *EA*, and bending, *EI*, rigidities with nanotube length are shown in Fig. 2, for the cases of armchair (10, 10), zigzag (10, 0) and chiral of the family $\theta = 8.9°$ SWCNTs. The tensile, *EA*, and bending, *EI*, rigidities stabilize from a certain value of the nanotube length, which is always less than 20 nm, whatever the SWCNT type, chiral or non-chiral, the chiral angle and nanotube diameter. The tensile and bending rigidities are almost constant, with increasing *EA* and decreasing *EI* for small nanotube lengths. A similar evolution of the tensile and bending rigidities was observed for non-chiral SWCNTs by Papanikos et al. [38], who justify the evolution of the rigidities observed for small nanotube lengths by the small ratio between the nanotube length and its diameter.

Taking into account the fact that the CNTs currently synthesized have relatively high length to diameter ratio, numerical simulation of the mechanical behaviour of nanotubes with a small length to diameter ratio is not needed. For this reason, in the following, 20 nm was chosen as modelling length for numerical simulation.

#### 3.1.2. Effect of the chiral indices and chiral angles on the rigidities of SWCNTs

The stabilized values of both the tensile and bending rigidities (i.e. determined for L = 20 nm) were used for evaluation of the effect of the SWCNT chiral indices, *n* and *m*, and chiral angle, $\theta$, on their mechanical properties. The evolutions of the tensile, *EA*, and bending, *EI*, rigidities as a function of the chiral indices, *n*, for armchair and zigzag nanotubes, and as a function of the sum of chiral indices, $(n + m)$, for chiral nanotubes, are shown in Fig 3. The evolutions of the tensile and bending rigidities, for armchair, zigzag and chiral SWCNTs, are related to the chiral indices as follows: the tensile rigidity, *EA*, increases quasi-linearly with the chiral indices and the bending rigidity, *EI*, increases with the chiral indices according to a cubic power expression. The *EA* evolutions can be separated for armchair, zigzag and chiral SWCNTs. The same is true for *EI* evolutions. In order to analyze the evolution of tensile and bending rigidities with chiral angle, $\theta$, SWCNTs with the same sum of chiral indices $(n + m)$ were considered. Fig. 4 shows that the values of both rigidities, *EA* and *EI*, for the three families $(n + m)$ studied, decrease from the rigidity values obtained for zigzag SWCNTs ($\theta = 0°$), with a rate that becomes smaller as $\theta$ increases.

In order to clarify the trends shown in Fig. 3, the values of the rigidities as a function of the SWCNT diameter, $D_n$, are plotted in Fig. 5. It can be seen that the evolution of the tensile rigidity, *EA*, can be unified for all SWCNTs studied, and the same is true for the bending rigidity, *EI*. The quasi-linear trend for the case of tensile rigidity, *EA*, and close to a cubic power trend for the case of bending rigidity, *EI*, can be expressed as follows:

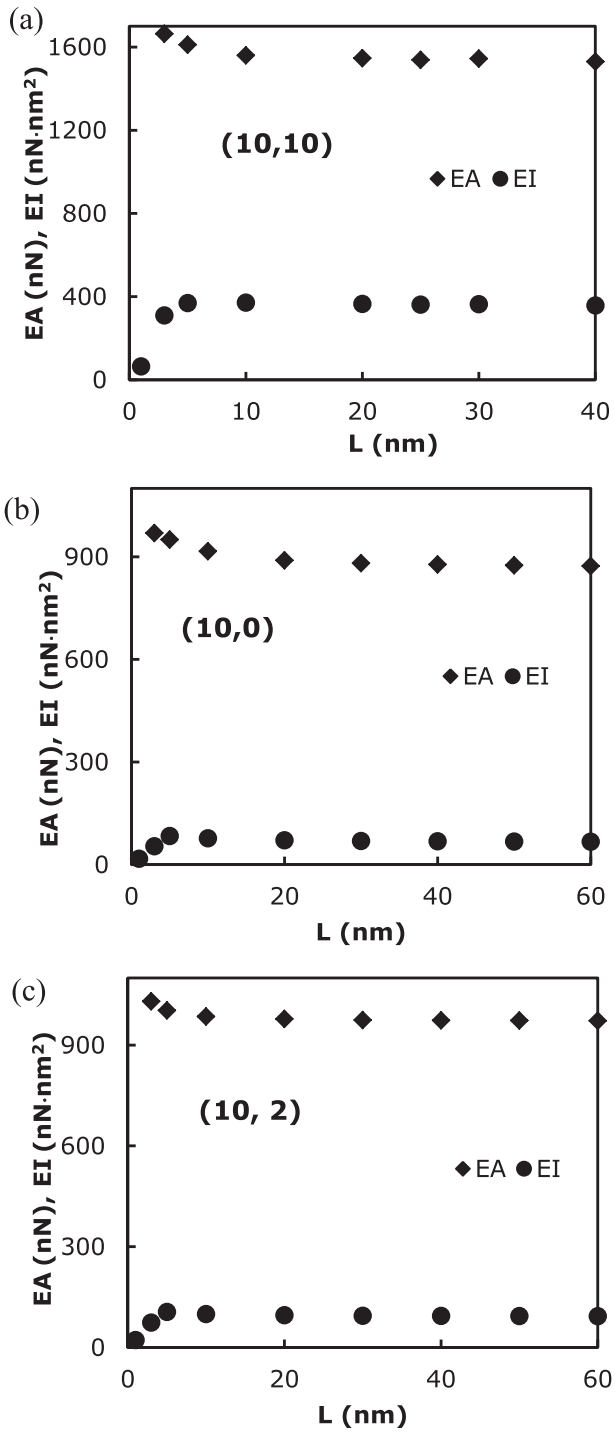


**Fig. 2.** Evolution of the tensile, *EA*, and bending, *EI*, rigidities with nanotube length, *L*, for (a) armchair (10, 10), (b) zigzag (10, 0) and (c) chiral (10, 2) SWCNTs.

$$EA = \alpha(D_n - D_0) \quad (22)$$

$$EI = \beta(D_n - D_0)^3 \quad (23)$$

These equations are of the same type as those previously proposed for non-chiral SWCNTs [38], but replacing the chiral index, *n*

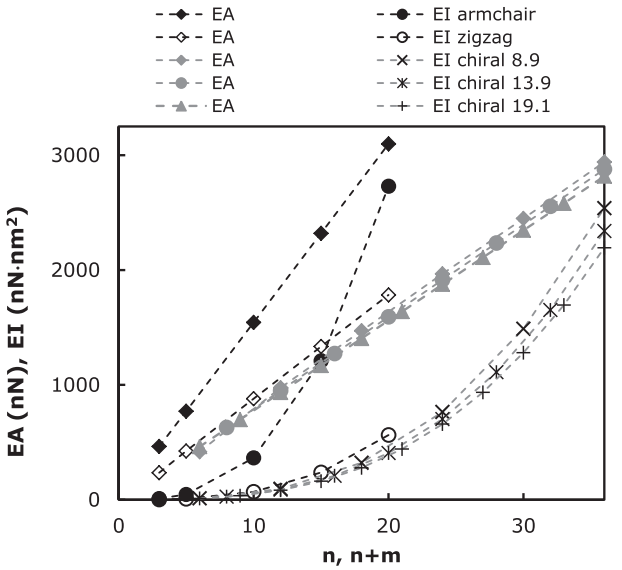


**Fig. 3.** Evolution of the tensile, *EA*, and bending, *EI*, rigidities of SWCNTs for armchair and zigzag, as a function of the chiral indices, n; and as a function of the sum of chiral indices, $(n+m)$, for three families $\theta = 8.9, 13.9, 19.1°$.

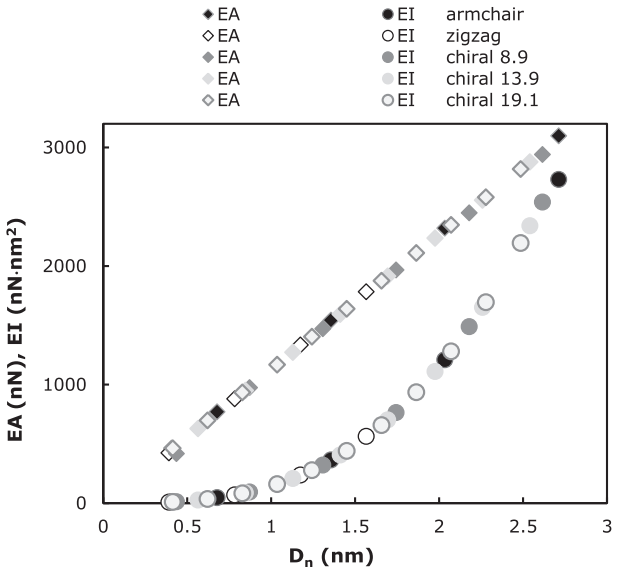


**Fig. 5.** Evolution of the tensile, *EA*, and bending, *EI*, rigidities as a function of the nanotube diameter, $D_n$ for armchair, zigzag and three families $\theta = 8.9, 13.9, 19.1°$.

by the SWCNT diameter, $D_n$. In this study [38], the evolutions of *EA* as a function of *n* can be separated for armchair and zigzag nanotubes; the same is valid for *EI* evolutions. The fitting parameters α, β and $D_0$ obtained in the current work, and those calculated based on the results of previous works ([38] and [52]) are given in Table 3. Fig. 6 (a) and (b) shows the values of *EA* and *EI* as a function of $(D_n - D_0)$ and $(D_n - D_0)^3$, respectively; the fitting lines from Eqs (22) and (23) are also shown.

Eqs. (22) and (23) allow unifying the behaviour of the SWCNTs regarding the evolution of rigidity with nanotube diameter and permit accurate determination of the rigidity values for chiral and non-chiral SWCNTs. The mean difference between the values of *EA*, obtained from Eq. (22), and the values obtained directly from FE analysis, is 0.65% for armchair, 0.56% for zigzag and 0.25% for chiral SWCNTs. The mean differences between the values of *EI* estimated by Eq. (23) and those obtained from FE analysis are 1.29% for armchair, 2.54% for zigzag and 0.66% for chiral SWCNTs. It is therefore possible to conclude that Eqs. (22) and (23) allow calculation, with sufficient accuracy, of the values of the tensile rigidity, *EA*, and bending rigidity, *EI*, whatever the type of SWCNT configuration in the range of nanotube diameters studied in the current work. Also, Eqs (22) and (23) permit fast assessment of the Young's modulus of any type of SWCNT, as shown in the next section.

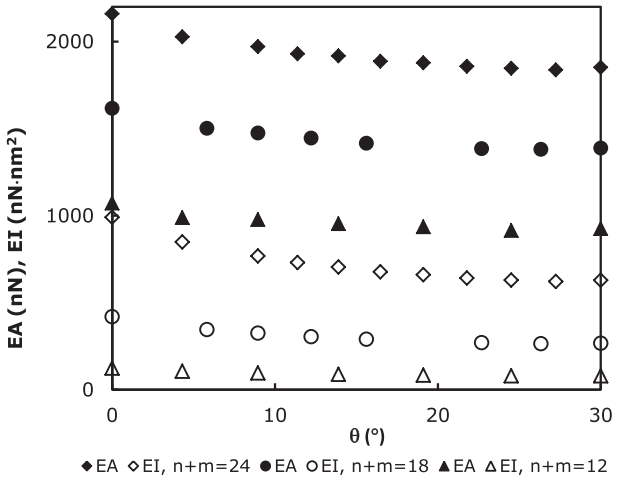


**Fig. 4.** Evolution of the tensile, *EA*, and bending, *EI*, rigidities as a function of the chiral angle, $\theta$ for three families of SWCNTs with $(n+m) = 12, 18, 24$.

### 3.2. Young's modulus of single-walled nanotubes

Eqs. (22) and (23) for the tensile and bending rigidities enable writing Eq. (21) as follows:

$$E = \frac{EA}{A} = \frac{\alpha(D_n - D_0)}{\pi t_n \sqrt{8\frac{\beta(D_n-D_0)^2}{\alpha} - t_n^2}} \tag{24}$$

This equation allows determination of the Young's modulus of any type of SWCNT, knowing the parameters of Table 3 and the wall thickness, $t_n$.

#### 3.2.1. Effect of the wall thickness on the calculation of the Young's modulus

Eqs. (21) and (24) show that the choice of the value of the wall thickness of the nanotubes has a direct impact on the calculation of the SWCNT Young's modulus. The scatter of the wall thickness value from 0.066 to 0.69 nm reported in the literature demonstrates the need to study the effect of the value considered on the Young's modulus, in order to discuss the FE results of the Young's modulus and enable comparison with the results reported in the literature.

**Table 3**
Fitting parameters $\alpha$, $\beta$ and $D_0$.

| Parameter | Current study[a] | Papanikos et al. [38] [b] | Chang&Gao [52] [b] |
|---|---|---|---|
| $\alpha$ (nN nm$^{-1}$) | 1131.66 | 1128.15 | 1141.3 |
| $\beta$ (nN nm$^{-1}$) | 143.48 | 142.54 | – |
| $D_0$ (nm) | $2.8\cdot10^{-7}$ | 0 | – |

[a] Includes armchair, zigzag and all types of chiral SWCNT studied.
[b] Includes armchair and zigzag SWCNT.

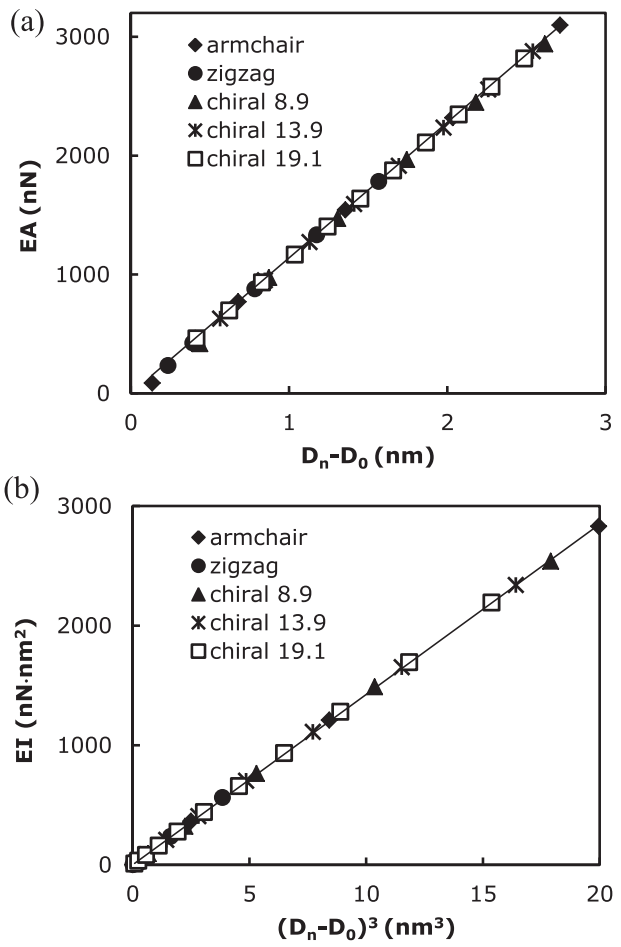


**Fig. 6.** Evolution of: (a) the tensile, *EA*, rigidity as a function of $(D_n - D_0)$ and (b) bending, *EI*, rigidity as a function of $(D_n - D_0)^3$. The results are represented by symbols and fitting trends by lines.

First, SWCNTs with different diameters were studied. Fig. 7 shows the Young's modulus determined by Eq. (24) as a function of the inverse of the nanotube wall thickness (for the range of $t_n$ values 0.06–0.69 nm), for the cases of the diameters of armchair SWCNTs shown in Table 1. The evolution of the Young's modulus as a function of the inverse of the wall thickness follows a quasi-linear trend over the whole range of thicknesses, for nanotubes with diameter $D_n \gtrsim 1.085$ nm. Such a linear trend was also reported by Tserpes and Papanikos [28] and Avila and Lacerda [39], although

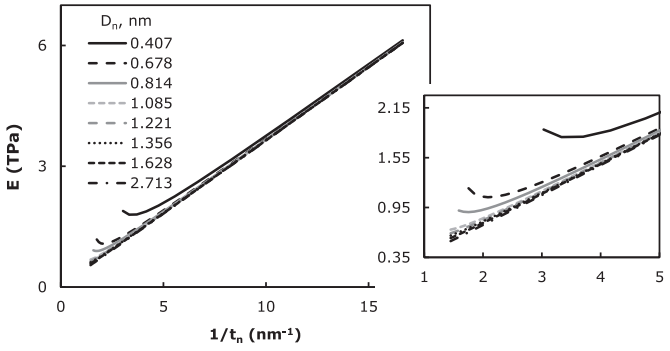


**Fig. 7.** Evolution of armchair SWCNTs Young's modulus with the inverse of the wall thickness for different nanotube diameters, according to Eq. (24).

only in one case of SWCNTs (8, 8) (diameter $D_n = 1.085$ nm). It is worth to notice that quasi-linear trends obtained here for different SWCNT diameters are nearly independent of $D_n$. This means that the SWCNTs Young's modulus behaviour as a function of nanotube diameter can be described by a single quasi-linear trend, for $D_n \gtrsim 1.085$ nm.

For the case of small nanotube diameters, $D_n \lesssim 1.085$ nm, the deviation from the quasi-linear trend is pronounced for smaller values of $1/t_n$, particularly when the nanotube wall thickness approximates to half of its diameter. The smaller the SWCNT diameter, the bigger is the deviation from the quasi-linear trend. For these cases, the SWCNT behaves as a solid cylinder, instead of a hollow tube, which influences the Young's modulus results. As long as the SWCNT wall thickness is equal to a half or less than its diameter, the Young's modulus becomes a quasi-linear function of the nanotube wall thickness. This is an interesting result, so far not reported in the literature to our knowledge, which allows unifying the elastic behaviour of CNTs, whatever their diameter or chirality.

Data from three main distinct modelling approaches –atomistic modelling, continuum modelling (CM) and nanoscale continuum mechanics modelling (NCM) – were chosen for comparison purposes. Seven studies, representing the atomistic approach, were considered: the *ab initio* approach of Kudin [9], the MD approaches of Yakobson [10], Zhang et al. [12], Cheng et al. [13] and Liew et al. [14], the TBMD models of Hernandez et al. [15] and Zhou [16]. Four cases of studies concerning the continuum mechanics approach reported in Refs. [18,20,22,23] were also considered. The remaining results were selected from the models developed employing the NCM approach: the equivalent truss model of Odegard et al. [26], six models, employing diverse kinds of spring elements: Meo and Rossi [30], Giannopoulos et al. [31], Mahmoudinezhad et al. [34], Natsuki et al. [35], Rafiee and Hendarhaei [36] and Parvaneh and Shariati [37], and seven models using beam elements: Papanikos et al. [38], Avila and Lacerda [39], Shokrieh and Rafiee [40], Her and Liu [41], Lu and Hu [42], Mohhamadpour and Awang [43].

Table 4 summarizes the results of the Young's modulus from the literature and the current results obtained from Eq. (24). The Young's modulus values were obtained for nanotube wall thicknesses, $t_n$, between 0.066 and 0.69 nm and are in the range 0.613–5.516 TPa. In order to facilitate comparison, the results given in Table 4 are plotted in Fig. 8. Fig. 8 shows that, for different wall thicknesses, the Young's modulus values obtained from Eq. (24) follow the trend of the Young's modulus reported in the literature, for a considerable number of approaches.

The current Young's modulus results are in particularly good agreement with those obtained in the studies basing on molecular dynamic modelling methods. The largest difference of 12.22%, observed with the TBMD model reported by Hernandez et al. [15], can be due to the fact that, in their work, the strain energy was calculated without taking the chiral angle into account. The difference of 6.90% in relation to the MD model of Liew et al. [14] can be due to the fact that empirical potentials were used by them. Empirical potentials are frequently not transferable to configurations different from those for which they were obtained. The smallest difference of 0.29% is found for the Young's modulus calculation performed with the MD model by Yakobson et al. [10], where non-linear behaviour of CNTs was considered, allowing correct identification of the strain energies.

Less good agreement is found when the Young's modulus results from the current study are compared with results from the CM models. The biggest difference (49.14%) is found with the Young's modulus results predicted by the analytical shell model of Kalamkarov et al. [20]. Comparison with the model reported by Gupta and Batra [23] shows a difference of 13.44%; this difference can be due to the fact that, in their work, the Young's modulus was evaluated

**Table 4**
Effect of the nanotube wall thickness on the Young's modulus results: comparison between the current results (Eq. (24)) and those reported in the literature.

| Reference | $t_n$, nm | Method | | $E$, TPa | | E, TPa (10, 10); $D_n = 1.356$ nm |
|---|---|---|---|---|---|---|
| Yakobson et al. [10] | 0.066 | Atomistic modelling | MD | 5.5 | Average value | 5.425 |
| Zhou et al. [16] | 0.074 | | TB model | 5.1 | Average value | 4.840 |
| Kudin et al. [9] | 0.089 | | *ab initio* | 3.859 | Average value | 4.027 |
| Zhang et al. [12] | 0.335 | | MD; Tersoff-Brenner potential | 1.08 | Converged value for zigzag SWCNTs | 1.101 |
| Liew et al. [14] | 0.335 | | MD: empirical potentials | 1.043 | (10, 10) SWCNT | 1.101 |
| Hernandez et al. [15] | 0.34 | | TBMD | 1.24 | (10, 10) SWCNT | 1.086 |
| Cheng et al. [13] | 0.34 | | MD coupled with NCM | 1.2 | Converged value for armchair SWCNTs | 1.086 |
| Pantano et al. [18] | 0.075 | CM | FE continuum shell model | 4.84 | Average value | 4.776 |
| Kalamkarov et al. [20] | 0.129 | | Analytical model: cylindrical network shell | 1.44 | – | 2.785 |
| Sears and Batra [22] | 0.134 | | Equivalent continuum tube | 2.52 | (16, 0) SWCNT | 2.682 |
| Gupta and Batra [23] | 0.34 | | Equivalent continuum tube | 0.964 | Average value for non-chiral and chiral SWCNTs | 1.086 |
| Odegard et al. [26] | 0.69 | NCM | Equivalent continuum modelling: truss elements | 0.49 | – | 0.601 |
| Meo and Rossi [30] | 0.34 | | FE model: non-linear springs and linear torsional spring elements | 0.926 | (10, 10) SWCNT | 1.086 |
| Giannopoulos et al. [31] | 0.34 | | 3D FE model: linear spring elements | 1.247 | Average value | 1.086 |
| Mahmoudinezhad et al. [34] | 0.34 | | 3D FE model: rotational spring elements | 0.85 | Converged value for armchair SWCNTs | 1.086 |
| Natsuki et al. [35] | 0.34 | | Analytical 2D model: spring elements | 0.61 | Average value | 1.086 |
| Rafiee and Heidarhaei [36] | 0.34 | | FE model: non-linear spring elements | 1.325 | Converged value for non-chiral SWCNTs | 1.086 |
| Parvaneh and Shariati [37] | 0.34 | | Structural mechanics model: springs and non-linear connectors | 1.170 | (22, 0) SWCNT | 1.086 |
| Tserpes and Papanikos [28] | 0.147 | | 3D FE model: linear elastic beam elements | 2.377 | (8, 8) SWCNT | 2.447 |
| Papanikos et al. [38] | 0.34 | | 3D FE model: linear elastic beam elements | 1.072 | Converged average value | 1.086 |
| Avila and Lacerda [39] | 0.34 | | 3D FE model: elastic beam elements; RVE concept | 1.005 | Average value | 1.086 |
| Shokrieh and Rafiee [40] | 0.33 | | Analytical model: beam elements | 1.042 | Converged value for armchair SWCNTS | 1.117 |
| Her and Liu [41] | 0.34 | | FE model: nonlinear beam elements; Morse potential | 0.927 | (10, 10) SWCNT | 1.086 |
| Lu and Hu [42] | 0.34 | | 3D FE model: beam elements of elliptical-like cross section area; non-linear potential | 1.058 | Converged value for zigzag SWCNTs | 1.086 |
| Mohammadpour and Awang [43] | 0.147 | | FE model: nonlinear beam elements; Morse potential | 2.037 | (10, 10) SWCNT | 2.447 |
| Current work | 0.34 | | 3D FE model: linear elastic beam elements | 1.078 | Converged average value | 1.086 |

by using free vibration simulations. Only the shell continuum model implemented in the work of Pantano et al. [18], shows a small difference (0.33%).

The nanoscale continuum models, employing string elements for C–C bond simulation, show a considerable scatter of the Young's modulus results, due to the values of the spring constants and the spring type selection. Differences with the current Young's modulus calculations are 12.92% (for the Giannopoulos et al. model [31] with linear spring elements) and 44.79% (for the analytical 2D model of Natsuki et al. [35]). The use of the 2D model by Natsuki et al. can explain the highest difference obtained. The model of Parvaneh and Shariati [37] provides the smallest difference of 6.24%.

The Young's modulus values evaluated in the current study show a 19.02% difference with the results of the truss model of Odegard et al. [26]. The models using the equivalent beam approach provided the smallest differences in relation to the current results. The difference of 9.04% observed with respect to the model of Avila and Lacerda [39] can be due to the representative volume element (RVE) concept applied in their work. The use of the RVE implies the numerical simulation of small length SWCNTs, which can affect the Young's modulus calculations. The highest difference observed with the ECM approach is of about 17%, reported in Refs. [41,43], where a modified Morse potential function was applied to the potential energy representation.

In order to simplify comparison with the literature, Table 5 shows the same cases as Table 4, but in the form of the product $Et_n$, which is called the averaging Young's modulus. The product $Et_n$ evaluated with the present model is in a good agreement with most of the averaging Young's moduli found in the references chosen. A few discrepancies between the Young's modulus results available in the literature and the results of the current evaluation are due to different modelling approaches (MD, CM, NCM), potential functions, force fields constants, formulations for Young's modulus determinations, etc.

Finally, a comparison between the experimental results reported in the literature and those of the present study is shown in Table 6. The Young's modulus evaluated is in satisfactory agreement with the experimental results reported by Krishnan et al. [53], who used thermal vibrations of SWCNT to estimate the Young's modulus, and the results of Yu et al. [54] who used a direct tensile loading test of SWCNT.

### 3.2.2. *Effect of chiral indices and diameter on the Young's modulus of SWCNTs*

Finally, a study concerning the influence of the chiral indices on the SWCNT Young's modulus was carried out. The Young's modulus was calculated with Eq. (21). The evolution of the Young's modulus, $E$, with chiral indices, for non-chiral and three families of chiral SWCNTs studied, is shown in Fig. 9 (a). The Young's modulus of the

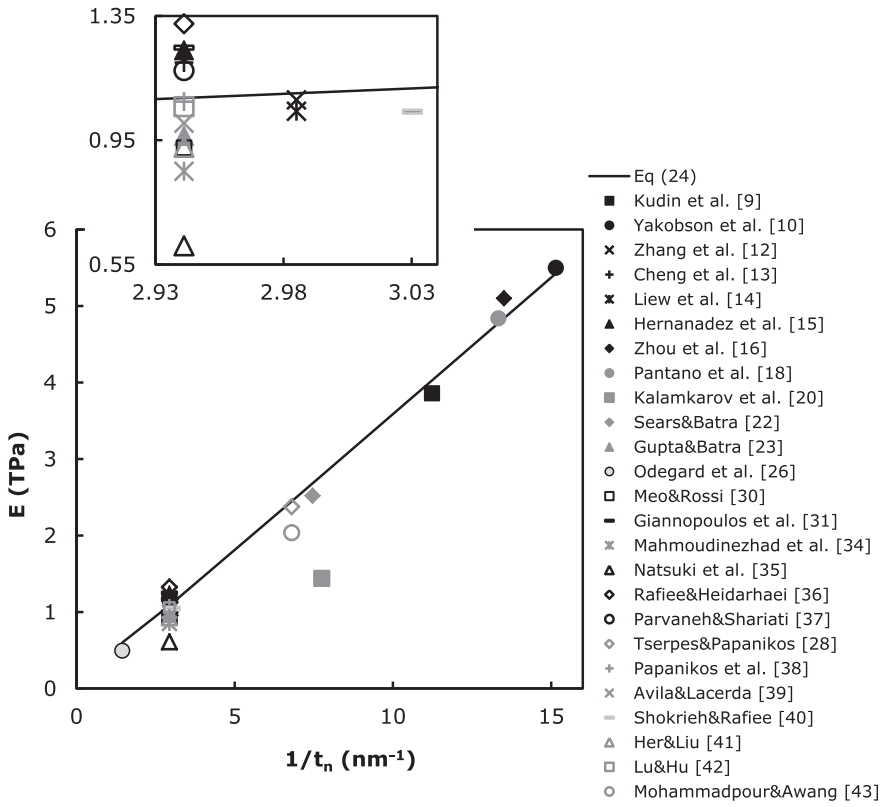


**Fig. 8.** Comparative study of the evolution of the Young's modulus of SWCNTs with the inverse of the wall thickness.

SWCNTs with small chiral indices $n,n + m \leq 10$ decreases with increasing $n$, for non-chiral, and $n+m$, for chiral nanotubes; afterwards the Young's modulus tends to stabilize at the value of about 1.1 TPa. In Fig. 9 (b), the results obtained for armchair and zigzag SWCNTs are compared with results available in the literature. For this purpose, literature Young's modulus results obtained for wall thickness $t_n = 0.34$ nm [38,41] and $t_n = 0.66$ nm [33] were chosen; also the work of Shen and Li [55] was considered, where the Young's modulus was deduced independently of the wall thickness. Fig. 9 (b) shows that the evolution of the Young's modulus reported by Papanikos et al. [38] is similar to that in the current work. The work of Her and Liu [41], where the equivalent beam approach was used, gives values of the Young's modulus for non-chiral SWCNTs, which are independent of the chiral indices in the range of $10 \leq n \leq 34$. The decrease of the Young's modulus with increase of $n$, for small chiral indices, $n = 3,4,5,6$, was observed by Ranjbartoreh and Wang [33]. Shen and Li [55] observed a decrease of the Young's modulus of armchair SWCNTs, even for $n > 10$, in a MD simulation study.

In order to clarify the trends shown in Fig. 9 (a), the Young's modulus results were represented as a function of the nanotube diameter in Fig. 10 (a). For all SWCNT configurations studied, the evolution of the Young's modulus can be described by the same trend: the Young's modulus decreases with increase of the nanotube diameter up to about $D_n = 1$ nm, then, with further increase in

**Table 5**
Comparative study of the averaging Young's modulus multiplied by the thickness, $Et_n$.

| Reference | $Et_n$, TPa nm |
|---|---|
| Current work | 0.369 |
| Kudin et al. [9] | 0.343 |
| Yakobson et al. [10] | 0.363 |
| Zhang et al. [12] | 0.362 |
| Cheng et al. [13] | 0.408 |
| Liew et al. [14] | 0.349 |
| Hernandez et al. [15] | 0.422 |
| Zhou et al. [16] | 0.377 |
| Pantano et al. [18] | 0.363 |
| Kalamkarov et al. [20] | 0.186 |
| Sears and Batra [22] | 0.338 |
| Gupta and Batra [23] | 0.328 |
| Odegard et al. [26] | 0.342 |
| Meo and Rossi [30] | 0.315 |
| Giannopoulos et al. [31] | 0.424 |
| Mahmoudinezhad et al. [34] | 0.289 |
| Natsuki et al. [35] | 0.207 |
| Rafiee and Heidarhaei [36] | 0.451 |
| Parvaneh and Shariati [37] | 0.399 |
| Tserpes and Papanikos [28] | 0.349 |
| Papanikos et al. [38] | 0.365 |
| Avila and Lacerda [39] | 0.342 |
| Shokrieh and Rafiee [40] | 0.344 |
| Her and Liu [41] | 0.315 |
| Lu and Hu [42] | 0.360 |
| Mohammadpour and Awang [43] | 0.299 |
| Literature average | 0.345 |

**Table 6**
Comparison between Young's modulus of SWCNTs estimated by the present method and experimental results in the available literature.

| Reference | $E$, TPa | |
|---|---|---|
| Krishnan et al. [53] | 1.3(−0.4/+0.6) | Average value of SWCNTs with diameter in the range of 1.0–1.5 nm |
| Yu et al. [54] | 1.0 | Average value for SWCNTs |
| Current work | 1.078 | Stabilized value for SWCNTs (see Figs. 9 (a) and 10 (a)) |

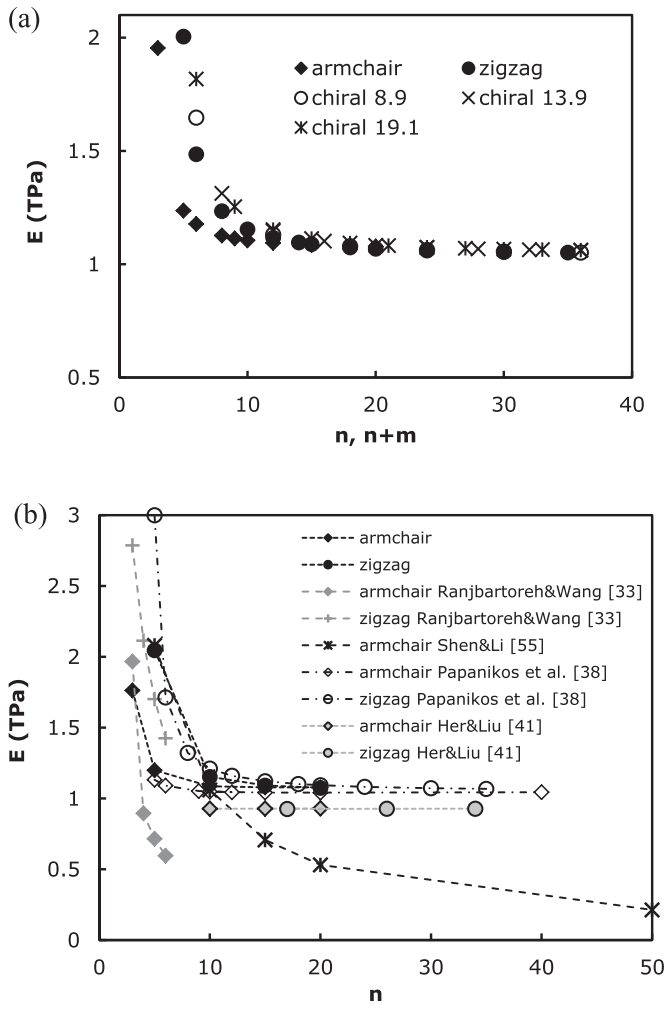


**Fig. 9.** (a) Evolution of the calculated Young's modulus of non-chiral and three families of chiral SWCNTs as a function of $n$ (for armchair and zigzag nanotubes) and $n+m$ (for chiral nanotubes); (b) comparison of the calculated Young's modulus results for armchair and zigzag nanotubes with those reported in the literature.

the nanotube diameter, the Young's modulus tends towards approximately the same value whatever the type of nanotube.

The results available in the literature, for a nanotube wall thickness of $t_n = 0.34$ nm were selected for comparison. Fig. 10 (b) plots the current Young's modulus results together with those from the literature, showing comparable trends of the Young's modulus evolution, i.e. the Young's modulus decreases for small SWCNT diameters and then becomes almost constant with increasing SWCNT diameter. Good agreement is observed with the results of the work of Papanikos et al. [38], where the modelling approach is similar to that of the current study. The same trend was reported by Zhang et al. [12] for armchair and zigzag nanotubes using MD simulation, in which the Young's modulus value tends to 1.0 TPa for armchair and 0.7 TPa for zigzag SWCNTs for diameters $D_n > 1.500$ nm. The results obtained in the molecular dynamic study of Shen and Li [55], and in the non-linear spring element model of Parvaneh and Shariati [37] show that the Young's modulus tends to 0.5 TPa for large nanotube diameters $D_n \geq 3.000$ nm.

Fig. 10 (c) also presents the current Young's modulus results plotted together with literature results. The literature results show a Young's modulus evolution that is almost constant over the whole range of nanotube diameters [56], although in same cases the Young's modulus increases slightly for small nanotube diameters [36,39,42].

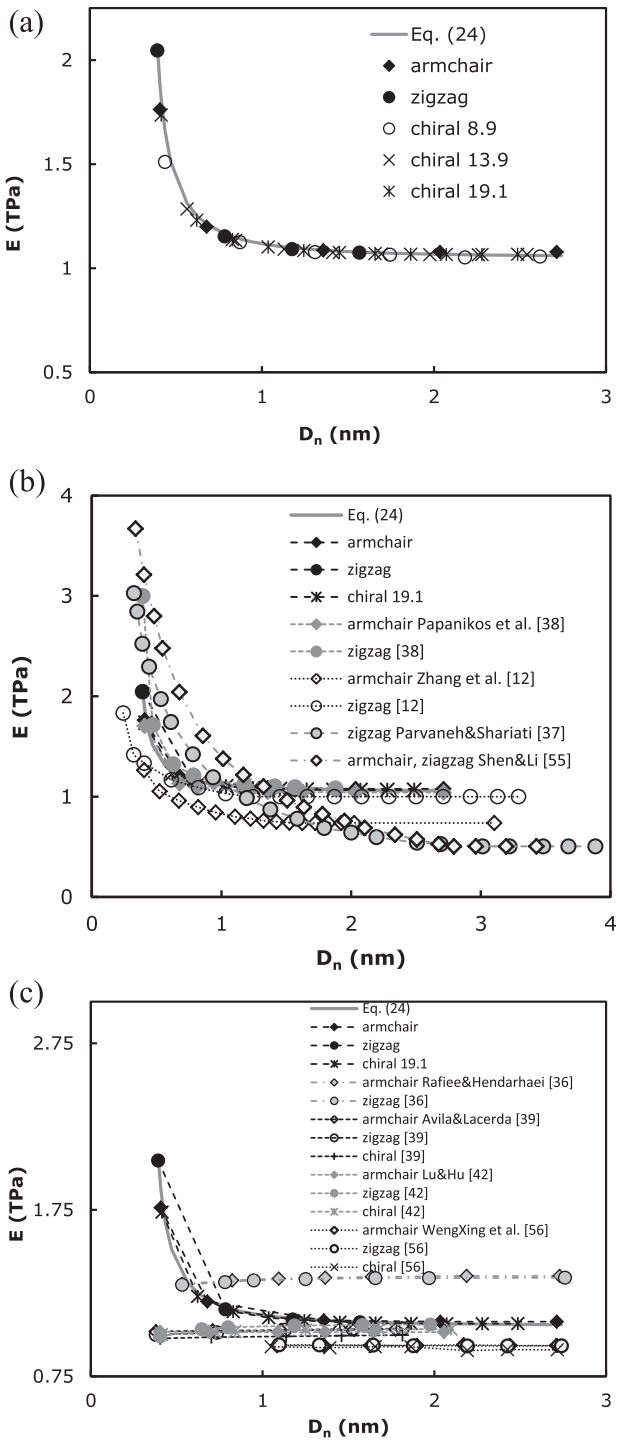


**Fig. 10.** (a) Evolution of the calculated Young's modulus of the SWCNTs with the nanotube diameter; (b) and (c) comparison of the calculated Young's modulus results with those reported in the literature.

Concerning the effect of SWCNT chirality on the Young's modulus, some authors reported similar values for armchair and zigzag SWCNTs [36,42,55]. In our study, and in agreement with results from the literature [38,56], the difference between the Young's modulus of armchair, zigzag and chiral SWCNTs, is also insignificant (see Figs. 9 and 10). A small difference between the Young's modulus for armchair and zigzag SWCNTs is reported by Zhang et al. [12], and for the three SWCNTs configurations by Avila and Lacerda [39] and Lu and Hu [42].

## 4. Conclusions

An equivalent beam approach has been used in order to carry out a systematic evaluation of the tensile and bending rigidities, and subsequently, Young's modulus of various SWCNT structures, namely non-chiral and families of chiral single-walled nanotubes over a wide range of chiral indices, nanotube lengths and diameters. The main conclusions of this comprehensive study are as follows:

- The evolution of the tensile rigidity, *EA*, as a function of the diameter, $D_n$, can be unified, for the SWCNTs studied; the same can be done for the bending rigidity, *EI*. Also, taking into consideration a given value of the wall thickness, the Young's modulus is about the same, whatever the chirality of the nanotube.
- An equation to correlate the tensile and bending rigidities of non-chiral and chiral SWCNTs with the nanotube diameter has been proposed. The accuracy of this relationship was tested using results available in the literature. A single equation is valid for armchair, zigzag and chiral SWCNTs, which allows easy evaluation of the Young's modulus.
- The Young's modulus values are proportional to the inverse of the wall thickness, for SWCNT diameters $D_n \gtrsim 1.085$ nm. For the case of small SWCNT diameters, deviation from this quasi-linear trend is observed, when the nanotube wall thickness is greater than a half of the nanotube diameter, $t_n \gtrsim 1/2D_n$. The quasi-linear trend of the Young's modulus as a function of the inverse of the wall thickness is in good agreement with the results of Young's modulus published by other authors.

## Acknowledgements

This research work is sponsored by national funds from the Portuguese Foundation for Science and Technology (FCT) via the projects PTDC/EME–TME/122472/2010 and PEst-C/EME/UI0285/2013 and by FEDER funds via “Programa Operacional Factores de Competitividade” – COMPETE, under the project CENTRO-07-0224_FEDER-002001 (MT4MOBI). All supports are gratefully acknowledged.

## References

[1] Robertson J. Realistic applications of CNTs. Mater Today 2004;7(10):46–52.
[2] Neubauer E, Kitzmantel M, Hulman M, Angerer P. Potential and challenges of metal-matrix-composites reinforced with carbon nanofibers and carbon nanotubes. Compos Sci Technol 2010;70(16):2228–36.
[3] Costa P, Silva J, Ansón-Casaos A, Martinez MT, Abad MJ, Viana J, et al. Effect of carbon nanotube type and functionalization on the electrical, thermal, mechanical and electromechanical properties of carbon nanotube/styrene–butadiene–styrene composites for large strain sensor applications. Compos Part B 2014;61:136–46.
[4] Zhang Y, Zhuang X, Muthu J, Mabrouki T, Fontaine M, Gong Y, et al. Load transfer of graphene/carbon nanotube/polyethylene hybrid nanocomposite by molecular dynamics simulation. Compos Part B 2014;63:27–33.
[5] Wang L, Zhang Z, Han X. In situ experimental mechanics of nanomaterials at the atomic scale. NPG Asia Mater 2013;5:e40.
[6] Kallesøe C, Larsen MB, Bøggild P, Mølhave K. 3D mechanical measurements with an atomic force microscope on 1D structures. Rev Sci Instrum 2012;83(2):023704.
[7] Rafiee R, Moghadam RM. On the modelling of carbon nanotubes: a critical review. Compos Part B 2014;56:435–49.
[8] Lu Q, Bhattacharya B. The role of atomistic simulations in probing the small scale aspects of fracture – a case study on a single-walled carbon nanotube. Eng Fract Mech 2005;72(13):2037–71.
[9] Kudin KN, Scuseria GE, Yakobson BI. C2F, BN and C nanoshell elasticity from ab initio computations. Phys Rev B 2001;64(23):235406.
[10] Yakobson BI, Brabec CJ, Bernholc J. Nanomechanics of carbon tubes: instabilities beyond linear response. Phys Rev Lett 1996;76(14):2511–4.
[11] Lu JP. Elastic properties of carbon nanotubes and nanoropes. Phys Rev Lett 1997;79(7):1298–300.
[12] Zhang HW, Wang JB, Guo X. Predicting the elastic properties of single-walled carbon nanotubes. J Mech Phys Solids 2005;53(9):1929–50.
[13] Cheng HC, Liu YL, Hsu YC, Chen WH. Atomistic continuum modelling for mechanical properties of single-walled carbon nanotubes. Int J Solids Struct 2009;46(7–8):1695–704.
[14] Liew KM, He XQ, Wong CH. On the study of elastic and plastic properties of multi-walled carbon nanotubes under axial tension using molecular dynamics simulation. Acta Mat 2004;52(9):2521–7.
[15] Hernandez E, Goze C, Bernier P, Rubio A. Elastic properties of C and BxCyNz composite nanotubes. Phys Rev Lett 1998;80(20):4502–5.
[16] Zhou X, Zhou J, Ou-Yang Z-C. Strain energy and Young's modulus of single-wall carbon nanotubes calculated from electronic energy-band theory. Phys Rev B 2000;62(20):13692.
[17] Ru CQ. Effective bending stiffness of carbon nanotubes. Phys Rev B 2000;62(15):9973.
[18] Pantano A, Parks DM, Boyce MC. Mechanics of deformation of single- and multi-wall carbon nanotubes. J Mech Phys Solids 2004;52(4):789–821.
[19] Muc A. Design and identification methods of effective mechanical properties for carbon nanotubes. Mater Des 2010;31(4):1671–5.
[20] Kalamkarov AL, Georgiades AV, Rokkam SK, Veedu VP, Ghasemi-Nejhad NM. Analytical and numerical techniques to predict carbon nanotubes properties. Int J Solids Struct 2006;43(22–23):6832–54.
[21] Chang TC. A molecular based anisotropic shell model for single-walled carbon nanotubes. J Mech Phys Solids 2010;58(9):1422–33.
[22] Sears A, Batra RC. Macroscopic properties of carbon nanotubes from molecular-mechanics simulations. Phys Rev B 2004;69(23):235406.
[23] Gupta SS, Batra RC. Continuum structures equivalent in normal mode vibrations to single-walled carbon nanotubes. Comput Mater Sci 2008;43(4):715–23.
[24] Wang Q. Effective in-plane stiffness and bending rigidity of armchair and zigzag carbon nanotubes. Int J Solids Struct 2004;41(20):5451–61.
[25] Arash B, Wang Q. A review on the application of nonlocal elastic models in modelling of carbon nanotubes and graphenes. Comput Mater Sci 2012;51(1):303–13.
[26] Odegard GM, Gates TS, Nicholson LM, Wise KE. Equivalent continuum modelling of nano-structured materials. Compos Sci Technol 2002;62(14):1869–80.
[27] Li C, Chou TW. Elastic moduli of multi-walled carbon nanotubes and the effect of van der Waals forces. Compos Sci Technol 2003;63(11):1517–24.
[28] Tserpes KI, Papanikos P. Finite element modeling of single-walled carbon nanotubes. Compos Part B 2005;36(5):468–77.
[29] Ghavamian A, Rahmandoust M, Öchsner A. On the determination of the shear modulus of carbon nanotubes. Compos Part B 2013;44(1):52–9.
[30] Meo M, Rossi M. Prediction of Young's modulus of single wall carbon nanotubes by molecular-mechanics based finite element modeling. Compos Sci Technol 2006;66(11–12):1597–605.
[31] Giannopoulos GI, Kakavas PA, Anifantis NK. Evaluation of the effective mechanical properties of single-walled carbon nanotubes using a spring based finite element approach. Comput Mater Sci 2008;41(4):561–9.
[32] Wernik JM, Meguid SA. Atomistic-based continuum modelling of the nonlinear behavior of carbon nanotubes. Acta Mech 2010;212(1–2):167–79.
[33] Ranjbartoreh AZ, Wang G. Consideration of mechanical properties of single-walled carbon nanotubes under various loading conditions. J Nanopart Res 2010;12(2):537–43.
[34] Mahmoudinezhad E, Ansari R, Basti A, Hemmatnezhad M. An accurate spring-mass model for predicting mechanical properties of single-walled carbon nanotubes. Comput Mater Sci 2012;62:6–11.
[35] Natsuki T, Tantrakarn K, Endo M. Prediction of elastic properties for single-walled carbon nanotubes. Carbon 2004;42(1):39–45.
[36] Rafiee R, Heidarhaei M. Investigation of chirality and diameter effects on the Young's modulus of carbon nanotubes using non-linear potentials. Compos Struct 2012;94(8):2460–4.
[37] Parvaneh V, Shariati M. Effect of defects and loading on prediction of Young's modulus of SWCNTs. Acta Mech 2011;216(1–4):281–9.
[38] Papanikos P, Nikolopoulos DD, Tserpes KI. Equivalent beams for carbon nanotubes. Comput Mater Sci 2008;43(2):345–52.
[39] Ávila AF, Lacerda GSR. Molecular mechanics applied to single-walled carbon nanotubes. Mater Res 2008;11(3):325–33.
[40] Shokrieh MM, Rafiee R. Prediction of Young's modulus of graphene sheets and carbon nanotubes using nanoscale continuum mechanics approach. Mater Des 2010;31(2):790–5.
[41] Her S-C, Liu S-J. Theoretical prediction of tensile behavior of single-walled carbon nanotubes. Curr Nanosci 2012;8(1):42–6.
[42] Lu X, Hu Z. Mechanical property evaluation of single-walled carbon nanotubes by finite element modeling. Compos Part B 2012;43(4):1902–13.
[43] Mohammadpour E, Awang M. Predicting the nonlinear tensile behavior of carbon nanotubes using finite element simulation. Appl Phys A 2011;104(2):609–14.
[44] Dresselhaus MS, Dresselhaus G, Saito R. Physics of carbon nanotubes. Carbon 1995;33(7):883–91.
[45] Barros EB, Jorio A, Samsonidz GG, Capaz RB, Souza Filho AG, Mendes Filho J, et al. Review on the symmetry-related properties of carbon nanotubes. Phys Rep 2006;431(6):261–302.
[46] Lau KT, Hui D. The revolutionary creation of new advanced materials – carbon nanotube composites. Compos Part B 2002;33(4):263–77.

[47] Melchor S, Dobado JA. CoNTub: an algorithm for connecting two arbitrary carbon nanotubes. J Chem Inf Comput Sci 2004;44(5):1639–46.
[48] Tang ZK, Sun HD, Wang J, Chen J, Li G. Mono-sized single-wall carbon nanotubes formed in channels of $AlPO_4$-5 single crystal. Appl Phys Lett 1998;73(16):2287.
[49] Rappe AK, Casemit CJ, Colwell KS, Goddard WA, Skiff WM. UFF, a full periodic-table force-field for molecular mechanics and molecular dynamics simulations. J Am Chem Soc 1992;114(25):10024–35.
[50] Gelin BR. Molecular modelling of polymer structures and properties. Cincinnati (OH): Hanser/Gardner Publishers; 1994.
[51] Cornell WD, Cieplak P, Bayly CI, Gould IR, Merz KM, Ferguson DM, et al. A second generation force-field for the simulation of proteins, nucleic acids and organic molecules. J Am Chem Soc 1995;117(19):5179–97.
[52] Chang T, Gao H. Size-dependent elastic properties of a single-walled carbon nanotube via a molecular mechanics model. J Mech Phys Solids 2003;51(6):1059–74.
[53] Krishnan A, Dujardin E, Ebbesen TW, Yianilos PN, Treacy MMJ. Young's modulus of single-walled nanotubes. Phys Rev B 1998;58(20):14013.
[54] Yu MF, Files BS, Arepalli S, Ruoff RS. Tensile loading of ropes of single wall carbon nanotubes and their mechanical properties. Phys Rev Lett 2000;84(24):5552–4.
[55] Shen L, Li J. Transversely isotropic elastic properties of single-walled carbon nanotubes. Phys Rev B 2004;69(4):045414.
[56] WenXing B, ChangChun Z, WanZhao C. Simulation of Young's modulus of single-walled carbon nanotubes by molecular dynamics. Phys B 2004;352(1–4):156–63.